Rotational Brownian Motion of Chromophores and Electric Field Effects in Polymer Films for Second-Order Nonlinear Optics

Lee-Yin Liu, Doraiswami Ramkrishna, and Hilary S. Lackritz*

School of Chemical Engineering, Purdue University, West Lafayette, Indiana 47907-1283

Received February 8, 1994; Revised Manuscript Received July 5, 1994®

ABSTRACT: Rotational dynamics of nonlinear optical chromophores embedded in amorphous polymer films were studied using second harmonic generation. Corona poling was used to orient the chromophores into the bulk noncentrosymmetric structure required to observe second-order nonlinearity. Electric field effects were examined by simultaneously measuring the second harmonic signal (during and following poling) and surface voltage decay (following poling). It is found that for short times the residual field following poling retards chromophore reorientation. A mathematical model that describes the rotational Brownian motion of chromophores in a polymer matrix is developed to simulate the field-dependent behavior. The electric field effects can therefore be deconvoluted from the Brownian motion to reveal information concerning local mobility in polymers. Further applications of the model in distinguishing the post-poling electric field effects and in computing the local free volume and viscosity are discussed. A first attempt is made to realize the contributions of the residual surface voltage, field-induced bulk charges, and thermally injected charges to the rotational motion of the chromophores. The magnitude of the local free volume and the local viscosity–temperature behavior in a doped poly(methyl methacrylate) system are estimated and compared with those predicted by the Doolittle–Williams–Landel–Ferry equation.

Introduction

Over the past decade, nonlinear optical (NLO) polymers have been used for optical applications such as waveguides,[1-3] optical modulators,[4] optical memory storage,[5] and holography.[6-8] Conventionally, inorganic crystals were used for these applications because of their high nonlinear optical performance. However, long times and delicate controls are required to grow crystals in the large sizes and optimized molecular structures needed for NLO devices.[9] Because of the versatility, ease of fabrication, and high optical grade of polymers, it has been shown that there are excellent potentials and benefits in developing nonlinear optical polymers.[10-12]

To obtain second-order NLO properties in a polymer system, suitable nonlinear dipolar chromophores must be doped into or functionalized onto the polymer. Electric field poling of the material is applied to achieve the bulk noncentrosymmetric ordering of the chromophores required for observing second-order nonlinear optical effects.[13-16] The magnitude of the second-order nonlinearity of a poled polymer, therefore, indicates the degree of the chromophore orientational order and can be utilized as a measurement for the local mobility and microscopic properties of the polymer system.[17-22]

Second harmonic generation (SHG), a second-order NLO process, is used to detect the small degrees of chromophore rotational motion in polymers.[15,23,24] Poling-induced chromophore orientation occurs in regions of sufficient local free volume and segmental mobility. The reorientation of the chromophores following poling undergoes rotational Brownian motion and is affected by the mobility of the polymer chains and the local free volume present in the vicinity of the chromophores. In this work, chromophore orientation is examined using SHG over a wide range of time and temperature, which vary the local mobility of polymers. With this technique, important information such as the temporal and thermal dependences of chromophore rotational diffusion, local free volume, and other properties of polymer microenvironment surrounding the chromophores can be realized.

Corona poling is used to supply the external electric field because of its frequent application in the optical area and its efficiency in creating a great electric field. However, the complicated electric field effects in corona-poled polymers are poorly understood. In this study, the electric field effects following poling are examined by *in-situ* surface voltage measurements. The surface voltage indicates that an electric field still persists in the poled polymer even though the poling process is terminated. The reorientation of the chromophores is therefore dependent upon not only the local mobility of the polymer matrix but also the residual electric field following corona poling.[25]

In this work, a dynamic model is developed to describe the rotational Brownian motion of chromophores affected by the electric field and the local mobility of a polymer matrix during and following poling. It assumes that the chromophores can only rotate within a limited space (a cone) because of the highly reduced mobility of polymer chains in the glass state. No rotational diffusion of the chromophores is allowed to occur at the boundary of the cone.[26,27] Since the reorientation of chromophores is more retarded if the cone size is smaller, the volume of the cone, as well as the wedge angle, can then be considered as an index of the local free volume (or local mobility) in a polymer system.

The electric field effect is quantified by calculating the dipole-field interaction in a uniform electric field for a first-order approximation. It is shown that the rotational diffusion coefficient following corona poling is about 2 orders of magnitude less than that during poling if the post-poling surface voltage effect is not deconvoluted from the rotational Brownian motion of the chromophores. The distinguishing of the electric field effect from the rotational Brownian motion has shown success in simulating the second-order NLO relaxation behavior and predicting the local free volume and viscosity of the polymer.

The rotational dynamic model is presented in the next section. In the experimental part, the second harmonic generation and surface voltage measurements are il-

* To whom correspondence should be addressed.

® Abstract published in *Advance ACS Abstracts*, September 1, 1994.

0024-9297/94/2227-5987$04.50/0

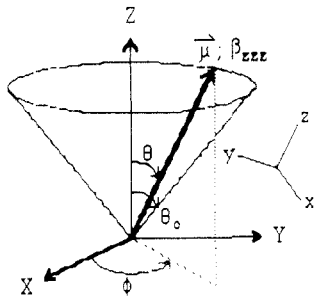

Figure 1. Diagram showing the wobbling of a chromophore within a cone with a wedge angle θ_0. The XYZ axes refer to the macroscopic coordinates with the Z axis parallel to the field-induced polar axis. The xyz axes are defined on the molecular frame with the z axis parallel to the dipole vector for the chromophore.

lustrated. The experimental results and the calculated data are discussed. A comparison between the $\chi^{(2)}$ relaxation and the surface voltage decay shows that the three governing factors dominate at different temperatures. The difference between the field-deconvoluted rotational diffusion coefficients during and following poling implies that there are other electric field effects involved. The local free volume and viscosity in 4-(dimethylamino)-4′-nitrostilbene-doped poly(methyl methacrylate) films are estimated and compared with those predicted by the traditional free volume model.

Theory

The study of chromophore orientation in a doped polymer film using SHG is important because it gives information about local polymer dynamics at the microscopic level, which is difficult to obtain by traditional methods such as specific volume or viscoelasticity measurements.[28-32] Three major factors that affect the rotation of chromophores are considered: the rotational Brownian motion, the electric field effects, and the restriction from the polymer host.

Rotational Motion of NLO Chromophores in a Polymer Host. Consider a one-dimensional dipolar chromophore with the orientation of its dipole moment at coordinates (θ,ϕ), where θ is the polar angle between the laboratory Z axis and the dipole vector and ϕ is the azimuthal angle (Figure 1). The Z axis is chosen as the poling-induced polar axis, which is essentially an infinite-fold rotational axis with an infinite number of mirror planes (∞mm or $C_{\infty v}$). Because of the $C_{\infty v}$ symmetry of the Z axis, the orientational distribution of the chromophore is independent of ϕ and only the θ-dependence is considered.

When an external electric field is applied across a doped polymer film, it exerts on the chromophore a torque, which forces the chromophore to orient along the field direction and results in a convectional diffusion of the chromophore. When the field is removed, reorientation of the chromophore occurs via rotational Brownian motion. However, not all the chromophores in the polymer matrix are allowed to rotate, especially when the temperature is well below the glass transition temperature T_g of the polymer system. Because the rotational mobility of the chromophores is mainly limited by the barrier system imposed by the polymer matrix, only those chromophores located in regions of sufficient local free volume (or local low density) have the greatest freedom to rotate. The rotational motion is confined in a range of polar angles if the size of the local free volume, as compared with that of the chromophore, is not large enough for the rotational diffusion to take place over all the angles. It is therefore assumed that the molecule is allowed to rotate within a cone with a maximum polar angle θ_0 (Figure 1) and no diffusion can occur at the boundary of the cone.[26,27]

Diffusion Equation. The rotational diffusion equation for a one-dimensional dipolar chromophore in an electric field is given by[25,33-38]

$$\frac{\partial p}{\partial \tau} = \frac{\partial}{\partial x}\left[(1-x^2)\frac{\partial p}{\partial x}\right] - (1-x^2)(bx+a)\frac{\partial p}{\partial x} + p(3bx^2+2ax-b) \quad (1)$$

where p is the probability density of finding a chromophore at a polar angle θ at time t. θ is the angle between the dipole moment and the field-induced polar axis (Z axis). Because of the $C_{\infty v}$ symmetry of the Z axis, no ϕ-dependence of the probability density is considered in eq 1. In eq 1, the angle and the time dependences of the probability density are written in terms of x and τ, respectively. The parameters x and τ are defined as

$$x \equiv \cos\theta \quad (2a)$$

and

$$\tau \equiv \int_0^t D\,dt \quad (2b)$$

where D is the rotational diffusion coefficient. The parameters a and b in eq 1 indicate the efficiency of the poling field in orienting the chromophore:

$$a \equiv \mu E/k_B T \quad (3a)$$

and

$$b \equiv \nu(g_1^0 - g_2^0)E^2/k_B T \quad (3b)$$

where μ is the permanent dipole moment and $\nu(g_1^0 - g_2^0)$ is the polarization anisotropy of the chromophore.[34,36-38] E is the strength of the poling field and $k_B T$ is the Boltzmann energy.

Definition of Initial Condition. (i) During Poling: Before any external electric field is applied across a fresh doped polymer system, the chromophores have a macroscopic centrosymmetric structure in the polymer host; i.e., the orientational distribution of the chromophores is random. The probability density of finding a molecule at any orientation is therefore identical:[9]

$$\text{I.C.:} \quad p_i(x)_{\text{during poling}} = 1/2 \quad (4)$$

(ii) Following Poling: In the work of Warchol and Vaughan[26] and that of Wang and Pecora,[27] a delta function is used as the initial orientational distribution of dipoles following poling. The delta function gives the ideal situation of the distribution but it is seldom the case in a poled polymer system. There will be a broader orientational distribution of the chromophores when the poling is terminated. Instead of the delta function, the calculated orientational distribution at the end of poling is chosen as the initial condition for the probability density following poling

$$\text{I.C.:} \quad p_i(x)_{\text{following poling}} \equiv p(x,\tau=\tau_{\text{off}})_{\text{during poling}} \quad (5)$$

where τ_{off} is the time when the applied field is removed.

Determination of Boundary Conditions. Because of the restriction of the polymer matrix, the chromophores can only rotate within a cone with a wedge angle θ_0. If the major contribution to the $\chi^{(2)}$ signal, the second-order nonlinear susceptibility, comes from the orientational

order of the chromophores confined in the cones whose cone axes are along the Z-direction, then only the rotational motion occurring in the range of $0 < \theta < \theta_0$ (or $x_0 < x < 1$, where $x_0 = \cos\theta_0$) is considered. Because the range of θ possesses the point $\theta = 0$ (or $x = 1$), which is a regular singular point of eq 1, it is necessary that the probability density be finite at this point. Therefore, the first boundary condition is

$$\text{B.C.1.:} \quad p(\theta{=}0,t) \equiv p(x{=}1,\tau) \text{ is finite} \tag{6}$$

The cone model assumes that the probability can only vary within the maximum polar angle θ_0, and no more change of probability can be observed outside θ_0; therefore the second boundary condition is given by

$$\text{B.C.2:} \quad \left.\frac{\partial p(\theta,t)}{\partial\theta}\right|_{\theta=\theta_0} = -\sin\theta_0 \left.\frac{\partial p(x,\tau)}{\partial x}\right|_{x=x_0} = 0 \tag{7}$$

Equation 7 states that the probability density flux at θ_0 is zero, implying that there is no diffusion through the boundary of the cone.

Because the changes of the cone size and orientation involve the motion of polymer chains, which is much slower than that of chromophores, the wedge angle and the orientation of a cone are assumed as constant, especially on a short time scale for a first-order approximation. The value of θ_0 in this model should be considered as a characteristic average value which represents a specific distribution of the cone size in the polymer system.

Solution of the Diffusion Equation. The rotational diffusion equation, eq 1, permits the separation of the time and space variables and can be solved to give an orientational distribution with the form

$$p(x,\tau) = \sum_{n=1}^{\infty} A_n \exp(-\lambda_n\tau)\, Y_n(x;\lambda_n,a,b) \tag{8}$$

where

$$Y_n(x;\lambda_n,a,b) = \sum_{k=0}^{\infty} f_k(\lambda_n,a,b)(1-x)^k \tag{9}$$

which is a Frobenius series.[39] The Frobenius series is used to confirm that the space function, $Y_n(x)$, is finite at B.C.1. The coefficient f_k can be determined from the recurrence relation which makes $Y_n(x)$ satisfy the eigenvalue problem of eq 1:

$$f_k = \frac{-1}{2k^2}\{[\lambda_n - k(k+2a-2b-1)]f_{k-1} + (a-3b)kf_{k-2} + bkf_{k-3}\};$$
$$(f_0 = 1, f_{-1} = f_{-2} = 0, k = 0, 1, 2, 3,\ldots) \tag{10}$$

λ_n is the nth eigenvalue. According to B.C.2, the space function $Y_n(x)$ satisfies the boundary condition

$$\left.\frac{\partial Y_n(x)}{\partial x}\right|_{x=x_0} = 0 \tag{11}$$

Substituting eq 9 into eq 11, the value of λ_n can be determined by solving

$$\sum_{k=1}^{\infty} kf_k(\lambda_n;a,b)(1-x_0)^{k-1} = 0 \tag{12}$$

A_n in eq 8 is the nth pre-exponential factor which can be computed at the initial condition. Because the solutions of the differential equation, eq 1, become an orthogonal system when eq 1 is multiplied by a weighting function $\xi(x)$, A_n can then be calculated by[40,41]

$$A_n = \int_{x_0}^{1} p_i(x)\,\xi(x)\,Y_n(x)\,dx \Big/ \int_{x_0}^{1} \xi(x) Y_n^2(x)\,dx \tag{13}$$

where

$$\xi(x) = \frac{1}{1-x_0^2}\exp\left\{-\left[\frac{b}{2}(x^2-x_0^2) - a(x-x_0)\right]\right\} \tag{14}$$

Once the initial condition is defined, the probability density at each point x (or θ) can then be numerically calculated on the τ-time scale. To plot the probability density on a real time scale, the temporal dependence of the rotational diffusion coefficient, D, must be known.

The $\chi^{(2)}$ value of the guest–host polymer system can be calculated by

$$\chi^{(2)}_{ZZZ} \approx N\boldsymbol{f}_Z(\omega)\,\boldsymbol{f}_Z(\omega)\,\boldsymbol{f}_Z(2\omega)\,\beta_{zzz}\langle\cos^3\theta\rangle =$$
$$N\boldsymbol{f}_Z(\omega)\,\boldsymbol{f}_Z(\omega)\,\boldsymbol{f}_Z(2\omega)\,\beta_{zzz}\int_0^{\theta_0}\cos^3\theta\; p(\theta,t;a,b,\theta_0,D)\sin\theta\,d\theta \tag{15}$$

where $\boldsymbol{f}$ is the local field factor, which is a function of the frequency of the optical field, ω. N is the number of doped NLO chromophores which are allowed to rotate. β_{zzz} is the second-order polarizability of the chromophore.[9,14]

From eq 15, it can be seen that the value of $\chi^{(2)}$ is dependent on the parameters a, b, θ_0, and D. The parameters a and b represent the electric field effect on the orientation of the chromophores. The wedge angle, θ_0, is an index of the polymer restriction. The rotational diffusion coefficient, D, indicates the relaxation rate through rotational Brownian motion. It will be shown that only the parameter D is allowed to be adjustable in this model, and the values of other parameters can be determined from experimental data. Therefore, this model gives an easy but strict method in simulation using only one variable. This strictness makes this model capable of predicting local molecular relaxation behavior and separating each individual contribution of electric field effects, polymer restriction, and Brownian motion to the $\chi^{(2)}$ property.

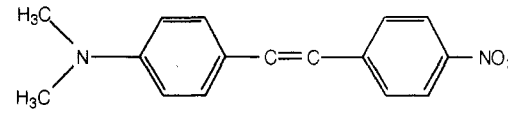

Figure 2. Chemical structure of 4-(dimethylamino)-4′-nitrostilbene (DANS).

Experimental Techniques

Sample Preparation and Characterization. Guest–host polymer systems were chosen as the first type of polymer systems for examining the rotational dynamic model. The host polymer was poly(methyl methacrylate) (PMMA) (Polysciences, Inc.) with a molecular weight of 75 000. The chromophore, 4-(dimethylamino)-4′-nitrostilbene (DANS) (Kodak) was used as received. The structure of DANS is shown in Figure 2. The relatively rigid, rodlike shape and high β value make DANS a good probe for sensing the local mobility of the polymer system.

PMMA doped with 4 wt % DANS was prepared by dissolving 10 wt % of solid in spectroscopic grade chloroform. The polymer solution was mixed well and filtered through a 5-μm filter. The solution was then spin coated onto indium tin oxide (ITO) coated glass slides to form uniform thin polymer films.

The films were dried carefully under identical conditions to remove as much solvent as possible. Ultraviolet and visible (UV–vis) spectroscopy (Perkin-Elmer) was used to identify the absorption range of the polymer films. The spectrum of PMMA

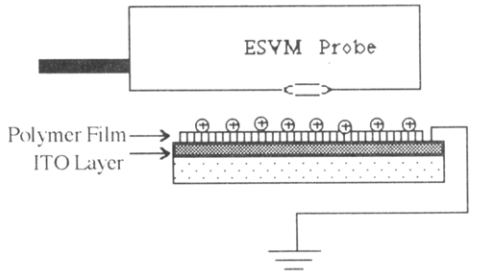

Figure 3. Diagram of surface voltage measurement. The surface voltage on the polymer film is measured by the electrostatic voltmeter (ESVM) probe following corona poling.

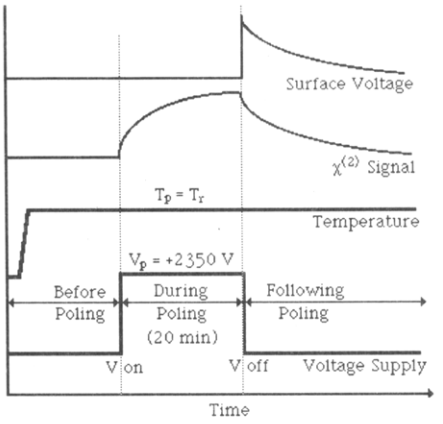

Figure 4. Diagram of the experimental procedure. The temperature is raised to the poling temperature, T_p, before poling and remains constant throughout the whole experiment. T_r, which indicates the temperature following poling, is equal to the poling temperature. The poling voltage, V_p, is 2.35 kV for all SHG measurements. Typical $\chi^{(2)}$ (during and following poling) and surface voltage curves (following poling) are also shown in the diagram.

doped with DANS shows absorption peaks at 430 and 300 nm, respectively. The glass transition temperature of PMMA doped with 4 wt % DANS was measured by differential scanning calorimetry (DSC) (10 °C/min) to be approximately 88 °C. The thickness of the polymer films measured using profilometry (Tencor Instrument, Alpha-Step 200) was about 3.8 μm.

Instrumentation. A p-polarized coherent light with a wavelength of 1064 nm was generated by a Q-switched Nd:YAG laser (Continuum NY61-10, pulse width ≈ 7 ns, intensity < 2 mJ/pulse, 10 Hz). The laser beam was split into two beams so that the sample and the 2-methyl-4-nitroaniline (MNA) reference were measured simultaneously. The reference was used to monitor the laser power, and the second harmonic intensity from the reference was used in calculating the relative $\chi^{(2)}$ values of the sample. The incident angle was fixed at 67° (measured from the normal vector of the sample surface to the incident beam) for all measurements so that comparisons could be made among different samples. The transmitted beam was filtered with a monochromator so that only the second harmonic signal at 532 nm was detected by a photomultiplier. The signal was triggered and averaged by an integrated boxcar analyzer and then digitized and collected by a Sun IPC workstation.

The dc electric field across the sample was generated by corona poling.[42] An insulated tungsten needle was mounted perpendicular to the film surface with an air gap of about 1 cm. The poling process was performed in a closed environment under a dry nitrogen atmosphere.

The *in-situ* surface voltage following poling was measured with an electrostatic voltmeter (ESVM). The ESVM probe was placed in front of the sample surface with an air gap of about 3 mm (Figure 3). The detected voltage was digitized by an electrometer and collected by the Sun workstation.

Procedure. Figure 4 shows a diagram of the experimental procedure. Before poling, a fresh sample was heated to the poling temperature, T_p. The temperature was maintained at T_p over 1 h. The temperature was kept constant throughout the entire experiment.

At time zero, the laser was turned on. The transmitted light was collected to obtain a baseline for the second harmonic intensity. After 300 s, an external dc electric field was applied across the sample using corona poling. The poling voltage, V_p, was kept constant during poling. The corona current was maintained at less than 1 μA. The poling process was allowed to continue for 20 min to obtain the equilibrium signal. The ESVM probe was then placed in front of the sample surface immediately when the poling voltage was shut down. The surface voltage and the second harmonic intensity were measured at the same time following poling.

Results and Discussion

In this section, the experimentally observed $\chi^{(2)}$ signals and the calculated data are compared. It is found that the dynamic model, in which the rotational Brownian motion, the electric field effects, and the polymer restriction are considered, has been successful in predicting the temporal dependence of the $\chi^{(2)}$ signal in a guest–host polymer system. The residual electric field effects are found to increase the short-term stability of the $\chi^{(2)}$ signal for a corona-poled NLO polymer.

Determination of Parameters. This rotational dynamic model contains four parameters: a ($=\mu E/k_BT$), b ($=\nu(g_1^0 - g_2^0)E^2/k_BT$), θ_0 (wedge angle of the cone), and D (rotational diffusion coefficient). The parameter a is obtained from surface voltage measurements. Assuming that the surface voltage generates a uniform electric field across the polymer film, the parameter a is related to the surface voltage by

$$a \equiv \frac{\mu E}{k_B T} \cong \frac{\mu (V/L)}{k_B T} \tag{16}$$

where V is the surface voltage and L is the thickness of the film (measured by profilometry). In eq 16, the local dc field factor is assumed about equal to 1.[9]

The value of the parameter b can be calculated by comparing the maximum $\chi^{(2)}$ signals obtained at different poling temperatures. A new parameter R_b is defined as

$$R_b \equiv \frac{\chi^{(2)}_{max}|_{T_p > T_g}}{\chi^{(2)}_{max}|_{T_p = T_g}} \tag{17}$$

where $\chi^{(2)}_{max}|_{T_p>T_g}$ and $\chi^{(2)}_{max}|_{T_p=T_g}$ are the maximum $\chi^{(2)}$ values measured at the poling temperature T_p greater than T_g and that equal to T_g, respectively. Because polymer chains begin to exhibit global or large-scale segmental motion at or above T_g, it is assumed that the rotation of doped chromophores undergoes little restriction from polymer chains and takes place over all the possible angles at or above T_g.[43] Therefore, the wedge angle, θ_0, becomes π. Assuming that all the chromophores are allowed to rotate above T_g (N, the number of active chromophores, is constant) and the temperature dependences of the local field factor f and β are both insignificant, then according to eq 17 R_b can be rewritten as

$$R_b = \frac{\langle \cos^3\theta \rangle_{T_p}}{\langle \cos^3\theta \rangle_{T_g}} = \frac{\int_{-1}^{1} p_\infty(x;\theta_0=\pi,a_p,b_p)x^3\,dx}{\int_{-1}^{1} p_\infty(x;\theta_0=\pi,a_g,b_g)x^3\,dx} \tag{18}$$

where p_∞ is the probability density at infinite τ during poling. The parameters a_p, b_p and a_g, b_g are parameters a and b at the specified poling temperature T_p and T_g, respectively. The diffusion coefficient, D, does not appear

in eq 18 because only the equilibrium situation ($\tau \rightarrow \infty$) is considered here. If the polarization anisotropy, $\nu(g_1^0 - g_2^0)$, of the material is constant within this temperature range ($T_g \leq T \leq T_p$), then

$$b_p = b_g\left(\frac{a_p}{a_g}\right)\left(\frac{E_p}{E_g}\right) \tag{19}$$

where E_p and E_g are the electric fields measured at T_p and T_g, respectively. Since R_b, a_p, a_g, E_p, and E_g can be determined experimentally, there is only one unknown b_g in eq 18. Therefore, b_g can be calculated by numerically solving eq 18. Substituting the value of b_g into eq 3b, the magnitude of the polarization anisotropy can be estimated. For PMMA + 4 wt % DANS, the value of $\nu(g_1^0 - g_2^0)$ is about $1.04 \times 10^{-5} D/(V/cm)$.

The value of wedge angle, θ_0, is defined as π if the temperature is at or above T_g. The value of θ_0 below T_g can then be evaluated by the following method. If θ_0 is assumed to be only temperature dependent, the temperature dependence of $\chi^{(2)}$ can be rewritten in terms of θ_0.

$$\chi^{(2)}(T) = \chi^{(2)}(\theta_0) \tag{20}$$

Considering only the maximum $\chi^{(2)}$ to eliminate the undetermined diffusion coefficient, a ratio R_{θ_0} is defined as

$$R_{\theta_0} \equiv \frac{\chi^{(2)}_{max}|_{T_p<T_g}}{\chi^{(2)}_{max}|_{T_p=T_g}} = \frac{\chi^{(2)}_{max},\theta_0<\pi}{\chi^{(2)}_{max},\theta_0=\pi} \tag{21}$$

Substituting eq 15 into eq 21 and neglecting the temperature dependences of both the local field factors f and β, R_{θ_0} can be expressed as

$$R_{\theta_0} = \frac{N(\theta_0)\langle\cos^3\theta\rangle_{\theta_0}}{N(\pi)\langle\cos^3\theta\rangle_{\pi}} \tag{22}$$

If N, the number of active chromophores, is assumed to be proportional to the volume of the cone (more chromophores are allowed to rotate if the size of the cone is larger), then

$$R_{\theta_0} = \frac{1-\cos\theta_0}{2}\frac{\int_0^{\theta_0} p_\infty(\theta;\theta_0,a,b)\cos^3\theta\sin\theta\,d\theta}{\int_0^{\pi} p_\infty(\theta;\theta_0=\tau,a_\pi,b_\pi)\cos^3\theta\sin\theta\,d\theta} \tag{23}$$

where a_π and b_π denote the parameters a and b when θ_0 equals π. Because the values of R_{θ_0}, a, and b have already been determined, θ_0 is the only unknown and can be calculated by solving eq 23. The value of θ_0, calculated from eq 23, is actually the apparent wedge angle $\langle\theta_a\rangle$ and is used in calculating the $\chi^{(2)}$ signals. The true wedge angle, used in estimating the local free volume, is related to $\langle\theta_a\rangle$ and is discussed in the following section. The values of the parameters a, b, and $\langle\theta_a\rangle$ at corresponding temperatures are listed in Table 1.

The rotational diffusion coefficient is obtained by changing the time scale (τ) of the calculated curve to fit the real-time experimental data. Figure 5 shows the experimental and calculated $\chi^{(2)}$ growth curves during poling. The values of a, b, and $\langle\theta_a\rangle$ listed in Table 1 were used to obtain the calculated curves. Because the surface voltage generated by corona poling approaches its equilibrium value faster than that of the polar order of

Table 1. Results of the Second Harmonic Generation and Surface Voltage Measurements and the Values of the Parameters Used in Simulation[a]

	T_p (°C)				
	75	83	88	95	101
$T_p - T_g$ (°C)	−13	−5	0	7	13
max $\chi^{(2)}$ (10^{-13} m/V)	9.3	9.7	10.7	7.7	7.5
ΔSV (V)	457.84	404.15	368.57	318.14	274.94
E (10^6 V/cm)	1.21	1.07	0.97	0.84	0.73
a	0.65	0.56	0.49	0.42	0.36
b	1.1	0.83	0.66	0.49	0.36
$\langle\theta_a\rangle$	44	46	180	180	180
D_p (10^{-4} s^{-1})	3.7	1.1	7.6	42	320
D_r (10^{-4} s^{-1})	2.57	9.5	23	75	178

[a] Polymer film thickness = 3.79 μm (measured using profilometer); permanent dipole moment μ of DANS = 7.6 D; volume of chromophore (DANS) = 207 Å^3 (calculated using the van der Waals volume); length of chromophore (DANS) = 14.2 Å (calculated); radius of the cross section of chromophore (DANS) = 2.15 Å (calculated).

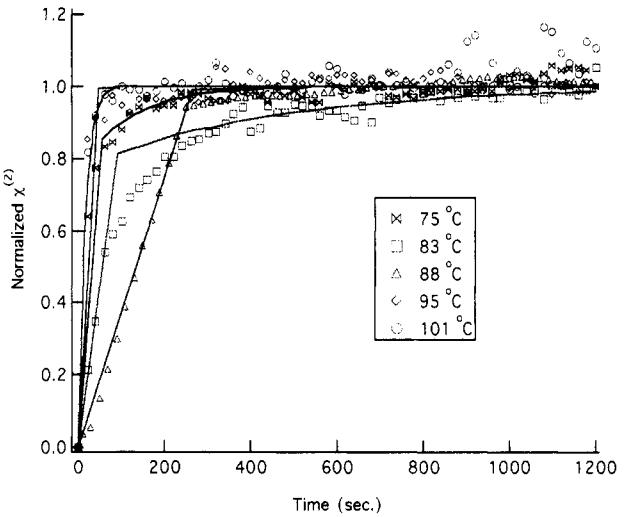

Figure 5. Experimental (markers) and calculated (solid lines) $\chi^{(2)}$ growth curves of the PMMA + 4 wt % DANS system during corona poling (+2.35 kV, in dry nitrogen).

chromophores,[44] the parameters a and b are assumed constant with respect to time throughout the entire poling period. A constant value of $\langle\theta_a\rangle$ is also used because the polymer system has been thermally treated to equilibrate at the poling temperature. The rotational diffusion coefficient during poling, D_p, is found to be constant and of order 10^{-4}–10^{-2} s^{-1} for temperatures ranging from 10 °C below to 10 °C above T_g (Table 1).

Figure 6 shows the experimental $\chi^{(2)}$ decay curves as well as the calculated ones following poling. Because the final temperature was the same as the poling temperature, the polymer matrix was at equilibrium if the applied electric field and the rotational motion of chromophores did not significantly perturb the configuration of the polymer chains. $\langle\theta_a\rangle$ is then assumed to be constant following poling and has the same value as it did during poling.

However, the surface voltage built up by corona poling does not vanish immediately when the poling process is terminated.[45] The post-poling surface voltage decay results in a residual electric field, which introduces a time dependence of parameters a and b. This residual electric field is found to affect the determination of the rotational diffusion coefficient following poling, D_r. Figure 7 shows the calculated $\chi^{(2)}$ decay curves with and without the residual electric field effect. Curve A, which represents the calculated $\chi^{(2)}$ decay without a residual electric field effect, was obtained by substituting zero values of both a

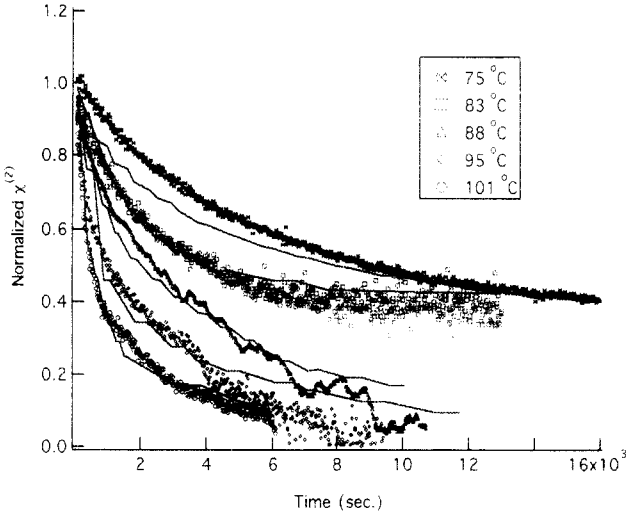

Figure 6. Experimental (markers) and calculated (solid lines) $\chi^{(2)}$ decay curves of the PMMA + 4 wt % DANS system following corona poling (+2.35 kV, in dry nitrogen).

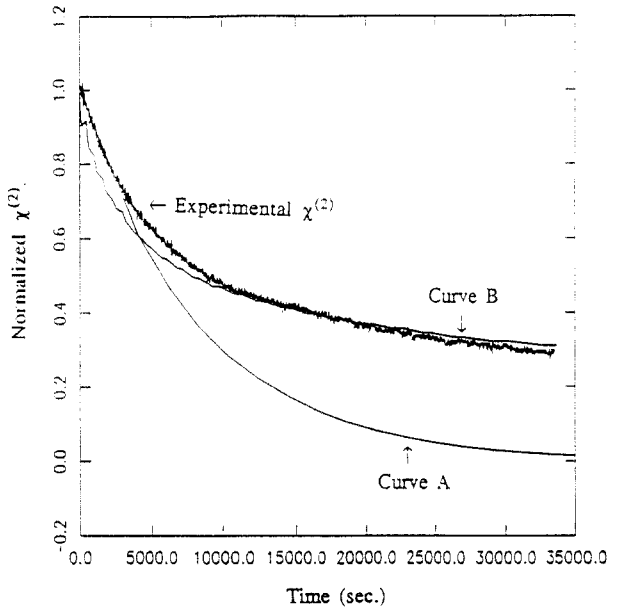

Figure 7. Experimental and calculated $\chi^{(2)}$ decay curves of the PMMA + 4 wt % DANS system at 75 °C (13 °C below T_g) following corona poling (+2.35 kV, in dry nitrogen). Curve A: calculated $\chi^{(2)}$ decay curve without considering the residual electric field effect. Curve B: calculated $\chi^{(2)}$ decay curve considering the residual electric field effect.

and b into the model. The deviation of curve A from the experimental data shows how greatly the residual electric field increases the stability of the $\chi^{(2)}$ signal. The diffusion coefficient D_r for curve A is found to be on the order 10^{-6} s^{-1}, which is 2 orders of magnitude less than D_p. This small value of D_r results from neglecting the residual electric field: the reorientation rate of chromophores is slowed down by the decreased diffusion coefficient rather than the residual electric field. The effect of the residual electric field is therefore implicitly involved in D_r.

To separate the contribution of the residual electric field to the chromophore reorientation, the time dependence of parameters a and b must be known. The *in-situ* surface voltage measurement gives

$$a(t) = \frac{\mu V(t)}{k_B T L} \tag{24a}$$

and

$$b(t) = \frac{\nu(g_1^0 - g_2^0)\, V^2(t)}{k_B T L^2} \tag{24b}$$

where $V(t)$ represents the surface voltage decay curve. However, the solution of the rotational differential equation, eq 1, does not allow parameters a and b to vary with time. Separation of variables fails to give a correct solution if the space parameters, including a and b, are also time-dependent. This mathematical difficulty can be overcome by dividing the entire time range into several small intervals. If each interval is short enough that the time dependence of a and b is negligible, eq 8 is still suitable for describing the rotational motion of chromophores within each time interval. Repeating the calculation in the subsequent interval and redefining the initial condition as the final condition of the previous interval, the reorientation process can be simulated over the whole time span of simulation.

There is another problem involved in separating the residual electric field effects. Because the surface voltage is measured on a real time scale, the diffusion coefficient D_r must be known prior to the application of experimental data in calculation, which is on the τ scale. The time dependence of the parameters $a(t)$ and $b(t)$ must be rewritten as $a(\tau)$ and $b(\tau)$ to keep the time scales consistent. The value of D_r is then determined by trial and error, and the numerical work iterates until a best fit is obtained. Curve B in Figure 7 shows the predicted result of the calculation, which describes the $\chi^{(2)}$ decay much better than curve A. Other calculated $\chi^{(2)}$ decay curves at different temperatures are shown in Figure 6. Values of D_r are given in Table 1. It is found that D_r is of the same order as D_p after the remaining surface voltage effect is deconvoluted. However, the values are still not close within experimental error. The field-induced bulk charges and the thermally excited charge injection may cause this difference.

Temperature Effect on the $\chi^{(2)}$ Signal. Figure 8 expresses the relationship between the maximum $\chi^{(2)}$ and temperature for the PMMA + 4 wt % DANS system. It also presents the variances of parameters a and θ_0 with temperature. Because the parameter a increases when the temperature decreases, the electric field becomes more effective in aligning the chromophores at lower temperatures. However, since the wedge angle (the freedom of rotation) has an opposite temperature dependence to that of parameter a, the polymer restriction prevents the alignment more prominently when the temperature is lowered. This indicates that there exists an optimum temperature at which a maximum value of $\chi^{(2)}$ can be obtained. The experimental data show that this optimum temperature is about T_g for the PMMA + 4 wt % DANS system.

At temperatures above T_g, although the rotational freedom has reached its maximum ($\theta_0 = \pi$), the increased Brownian motion breaks the alignment of the chromophores and thus decreases the $\chi^{(2)}$ value. When the temperature is lower than T_g, the $\chi^{(2)}$ signal is decreased by the polymer restriction even though the rotational driving force, a, is high.

This observation also implies that the assumptions made previously are suitable in the data analysis for the experiments performed in this work: (i) the applied electric field and the induced rotation of chromophores have little effect in distorting the conformation of the polymer chains; (ii) the wedge angle becomes π at T_g. If the strength of the applied field is so high that it produces enough dipole-

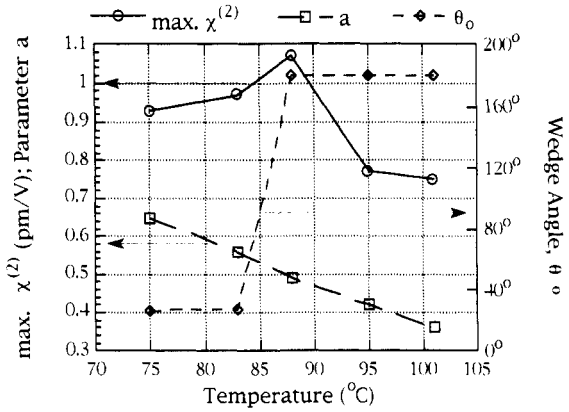

Figure 8. Temperature dependences of $\chi^{(2)}$, the parameter a, and the wedge angle θ_0 for the PMMA + 4 wt % DANS system (corona poled at +2.35 kV in a dry nitrogen atmosphere).

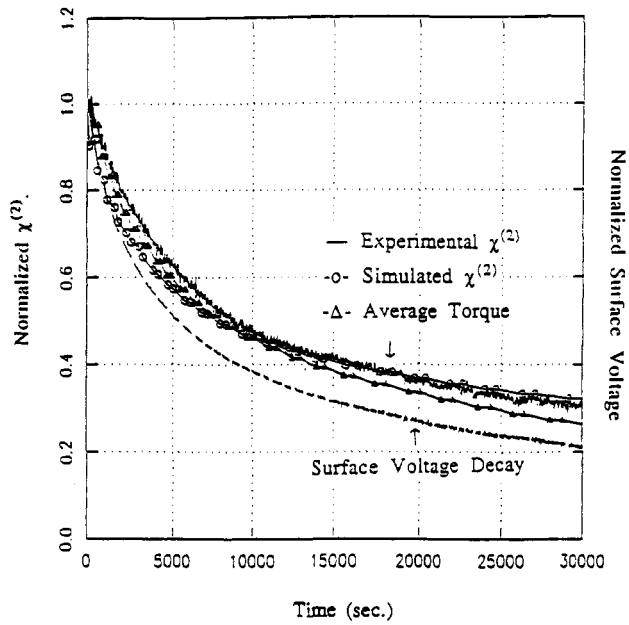

Figure 9. Surface voltage (- - -), $\chi^{(2)}$ ((—) experimental; (O) calculated), and average torque (Δ) decay curves of the PMMA + 4 wt % DANS system at 75 °C (13 °C below T_g) following corona poling (+2.35 kV, in dry nitrogen).

field interaction energy for the chromophores to break through the confinement of polymer chains, it is possible to observe the maximum $\chi^{(2)}$ signal at a temperature below T_g. This situation is insignificant for the electric field range used in this work. The occurrence of a maximum $\chi^{(2)}$ at T_g rather than other temperatures indicates that the polymer restriction, which strongly affects the $\chi^{(2)}$ signal at low temperatures, reaches its minimum at T_g and has no more significant change at higher temperatures. It is thus suitable to define T_g as the temperature at which the wedge angle, θ_0, becomes π, and therefore no larger value of θ_0 is available at higher temperatures.

Residual Electric Field Effects. Both the surface voltage decay and the $\chi^{(2)}$ relaxation, along with the calculated curves, for the PMMA + DANS films following corona poling are presented in Figures 9–11. The figures show that the surface voltage and the $\chi^{(2)}$ signal exhibit a similar but not identical relaxation rate. This indicates that the remaining surface voltage affects the $\chi^{(2)}$ decay, but other mechanisms such as the rotational Brownian motion also contribute to the $\chi^{(2)}$ relaxation. The calculated curve, which is derived by considering both the residual surface voltage effect and the Brownian motion, gives a better description of the $\chi^{(2)}$ relaxation.

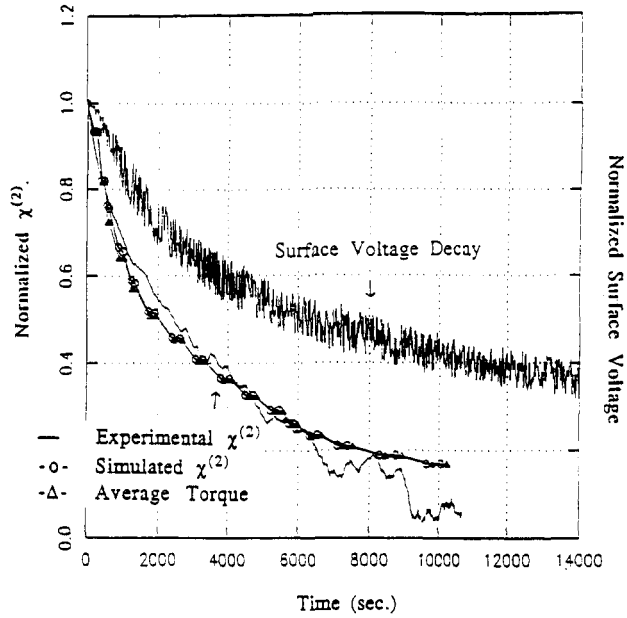

Figure 10. Surface voltage (- - -), $\chi^{(2)}$ ((—) experimental; (O) calculated), and average torque (Δ) decay curves of the PMMA + 4 wt % DANS system at 88 °C (T_g) following corona poling (+2.35 kV, in dry nitrogen).

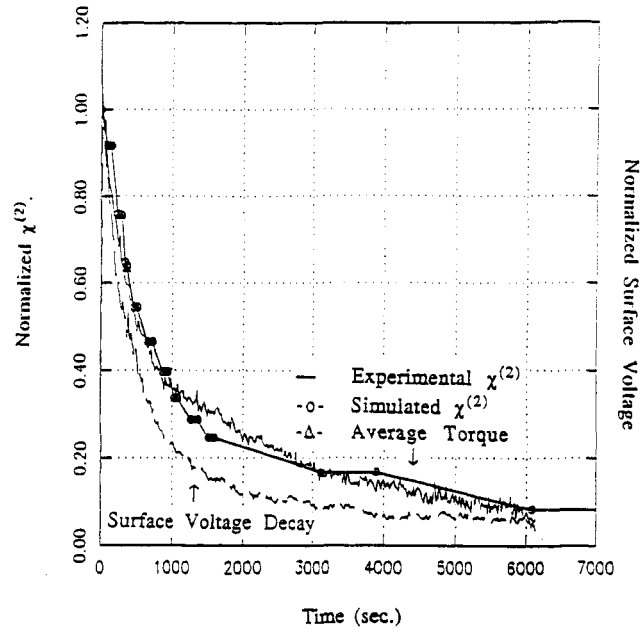

Figure 11. Surface voltage (- - -), $\chi^{(2)}$ ((—) experimental; (O) calculated), and average torque (Δ) decay curves of the PMMA + 4 wt % DANS system at 101 °C (13 °C above T_g) following corona poling (+2.35 kV, in dry nitrogen).

Figures 9–11 also show the calculated average torques acting on the chromophores following poling. It is interesting that the torque decays with a rate very close to that the $\chi^{(2)}$ signal. This implies that the $\chi^{(2)}$ decay is more related to the torque in the bulk rather than the surface voltage. The torque produced by an electric field on a dipole μ is given by[46]

$$\mathcal{T} = -\mu E \sin\theta \tag{25}$$

Since the field also polarizes the chromophore, there is an additional torque which comes from the interaction of the field and the induced polarization. The total torque on an individual chromophore is then given by

$$\mathcal{T} = -\mu E \sin\theta - E^2 \cos\theta \sin\theta \, \nu(g_1^0 - g_2^0) \tag{26}$$

where the term $\nu(g_1^0 - g_2^0)$ represents the difference between the polarizabilities along the parallel and the perpendicular axes of the chromophore.[34,36-38]

Assuming that there are no intermolecular interactions, the average torque $\langle \mathcal{T} \rangle$ on the whole assembly of the chromophores is

$$\langle \mathcal{T} \rangle = \int_0^{\pi} \mathcal{T}(\theta)\, p(\theta,t) \sin\theta \, d\theta \qquad (27)$$

where $p(\theta,t)$ is the orientational distribution function. Because of the polymer restrictions, only the rotation of the chromophores with orientation located between 0 and θ_0, the wedge angle of the cone, is significant; then

$$\langle \mathcal{T} \rangle = \int_0^{\theta_0} \mathcal{T}(\theta)\, p(\theta,t) \sin\theta \, d\theta + \langle \mathcal{T} \rangle_r \qquad (28)$$

where $\langle \mathcal{T} \rangle_r$ is the average torque on the chromophores outside the cone. Because the rotation of the chromophores outside the cone is not noticeable, $\langle \mathcal{T} \rangle_r$ can be assumed as a constant and contributing little to the time dependence of $\langle \mathcal{T} \rangle$. The orientational distribution of the chromophores varies with time through rotational Brownian motion and therefore can be calculated using eq 8. Introducing the parameters a and b in eqs 3a and 3b into eq 26 and defining a dimensionless torque $\Gamma \equiv \mathcal{T}/k_B T$, eq 28 can be rewritten as

$$\langle \Gamma \rangle = \int_{x_0}^{1} P(x,t)\,(a - bx)\,(1 - x^2)^{1/2}\, dx + \langle \Gamma \rangle_r \qquad (29)$$

where $x = \cos\theta$ and $x_0 = \cos\theta_0$. Assuming that there is a uniform distribution of the chromophores outside the cone, $\langle \Gamma \rangle_r$ can be determined by

$$\langle \Gamma \rangle_r = \frac{a}{4}\left[\pi - \theta_0 + \frac{\sin(2\theta_0)}{2}\right] + \frac{b}{6}\sin^3\theta_0 \qquad (30)$$

It is found in eq 30 that if parameters a and b vary with time (following poling), $\langle \Gamma \rangle_r$ will exhibit the same time dependence as a and b. Because the time dependence of a and b comes from the surface voltage decay, $\langle \Gamma \rangle_r$ has the same relaxation behavior of the surface voltage. $\langle \Gamma \rangle_r$ thus represents the part which is explicitly affected by the surface voltage of the average torque, $\langle \Gamma \rangle$.

The integral portion in eq 29, which involves the contribution of rotational Brownian motion to the average torque, results in the difference between the decay rates of the surface voltage and $\langle \Gamma \rangle$. Because the orientation of the chromophore is directly affected by the torque acting on it, the $\chi^{(2)}$ signal shows a decay rate closer to that of $\langle \Gamma \rangle$ rather than that of the surface voltage.

Figure 10 shows a faster $\chi^{(2)}$ decay than that of the surface voltage at T_g. It can been seen that the Brownian motion assists the $\chi^{(2)}$ relaxation. However, when the temperature is far below or far above T_g, a reverse situation is observed (Figures 9 and 11). At low temperature, the polymer restrictions become significant and confine the reorientation of the chromophores within a smaller space. The $\chi^{(2)}$ decay is thus retarded even though the surface voltage vanishes.

The slower $\chi^{(2)}$ relaxation, relative to the surface voltage decay, at high temperature may be caused by the thermally excited charge transport mechanism.[47-52] The surface-trapped charges are excited at high temperature and begin to inject into the bulk. The dissipation of the surface charges is thus accelerated and a faster decay is observed at high temperature. Moreover, if the injected charges are trapped again inside the bulk, those bulk-trapped charges will interact with the dipoles and affect the $\chi^{(2)}$ decay. Assuming that the interaction between the bulk charges and dipoles retards the reorientation of the chromophores, the $\chi^{(2)}$ signal will be stabilized by those charges. Since the charge injection increases the surface voltage decay but slows down the $\chi^{(2)}$ relaxation, a relatively slower $\chi^{(2)}$ decay, as compared to that of the surface voltage, is observed at high temperature.

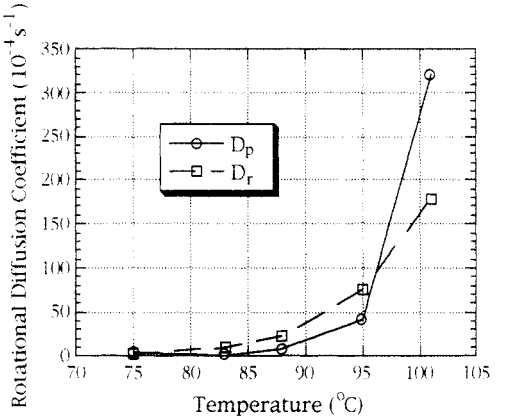

Figure 12. Temperature dependences of the rotational diffusion coefficients D_p (during poling) and D_r (following poling) for the PMMA + 4 wt % DANS system.

The temperature dependences of the rotational diffusion coefficients, D_p (during poling) and D_r (following poling), are shown in Figure 12. The values of D_p and D_r are expected to be the same if there is no post-poling electric field effect at constant temperature. However, if the remaining surface voltage decay is not considered in calculating the $\chi^{(2)}$ relaxation following corona poling, the magnitude of D_r is found to be about 2 orders less than that of D_p. Once the residual electric field effects are separated from the $\chi^{(2)}$ relaxation, both D_p and D_r should be the same and describe only the magnitude of the rotational Brownian motion of the chromophores. Data shown in Figure 12 were obtained by considering the surface voltage decay in the calculation.

It can be seen in Figure 12 that D_p and D_r are of the same order. The difference between D_p and D_r may come from the effect of the bulk charges induced by the poling field or by the thermally excited injection of the surface-trapped charges.[47-49,51-53] These two types of bulk charges, classified by the origins, seem to dominate at different temperature ranges and have opposite effects in affecting the magnitude of the rotational diffusion coefficients. The field-induced bulk charges, which have opposite polarity to that of the surface charges, cancel out a part of the efficiency of surface charges in retarding the Brownian motion of the chromophores and therefore increase the diffusion coefficient following poling ($D_r > D_p$, as shown in Figure 12 at temperature near T_g = 88 °C). At higher temperatures, a large-scale charge injection is excited. The injected charges, whose polarity is the same as the surface charges, not only eliminate the opposite effect of the induced charges but also assist the maintenance of the alignment of the chromophores. Therefore, a decreased diffusion coefficient is observed ($D_r < D_p$, Figure 12, T = 101 °C).

Estimation of Local Free Volume. In a real polymer system, the orientation of the cone can be in any direction instead of a single Z-direction (polar axis). Considering a cone which is tilted an angle α away from the Z-direction (Figure 13) and defining the probability density of finding this kind of cone as $p_c(\alpha)$, then in an amorphous polymer

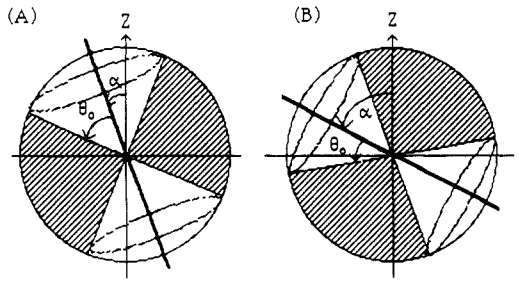

Figure 13. The orientation of the cone axis is tilted and angle α away from the Z axis.

Table 2. Values of the Apparent Wedge Angle ($\langle\theta_a\rangle$), True Wedge Angle (θ_0), Cone Volume (V_c), and Local Free Volume (V_0) at Different Temperatures

	T_p (°C)				
	75	83	88	95	101
$\langle\theta_a\rangle$ (deg)	44	46	180	180	180
θ_0 (deg)	26.4	27.6	180	180	180
V_c (Å^3)	668	697	1499	1499	1499
V_0 (Å^3)	462	491	1293	1293	1293

matrix the orientation of the cone is equally distributed and p_c is azimuthal-independent. Therefore

$$p_c(\alpha) \propto \sin\alpha \tag{31}$$

The rotational diffusion of the chromophores within those cones can go further down to a larger polar angle $\theta_a = \theta_0 + \alpha$ instead of θ_0, and it seems to the observer that the wedge angle (or the size of the cone) is increased. What is observed is the averaged apparent angle $\langle\theta_a\rangle$ rather than the true wedge angle θ_0. Since $\langle\theta_a\rangle$ is larger than θ_0, the cone volume will be overestimated if $\langle\theta_a\rangle$ is used as θ_0 in calculations.

To resolve this problem, it is necessary to further categorize those tilted cones into two cases and investigate the chromophore rotational motion in each case. Case A: the tilted cone still contains the Z-axis, which means the range of θ still has the regular singular point of eq 1, $\theta = 0$ (Figure 13A). The range of the tilted angle α is therefore between 0 and θ_0 to satisfy this requirement. Case B: the Z-axis only passes through the acme of the cone. The regular singular point is not included in the cone (Figure 13B).

In both cases, the differential equation which describes the rotational diffusion of the chromophores remains the same as eq 1. However, the boundary conditions must be redefined. Because the regular singular point, $\theta = 0$, is included in case A, the B.C.'s for case A are given by

$$\text{B.C.1:} \quad p(\theta = 0,t) \equiv p(x=1,\tau) \text{ is finite} \tag{32}$$

and

$$\text{B.C.2:} \quad \left.\frac{\partial p(\theta,t)}{\partial\theta}\right|_{\theta=\theta_a} = 0, \qquad \theta_a = \theta_0 + \alpha \tag{33}$$

which are the same as the ones defined previously (eqs 6 and 7) if the tilted angle α is zero. Therefore, the differential equation can be solved by the same procedure and the probability density p has the same form as eq 8. The cones at a given α can then be viewed as forming a larger cone with an apparent angle θ_a, and the average value of θ_a is related to θ_0 by

$$\langle\theta_a\rangle = \int_0^{\theta} \theta_a p_c(\alpha)\, d\alpha = \theta_0 + \frac{\sin\theta_0 - \theta_0\cos\theta_0}{1 - \cos\theta_0} \tag{34}$$

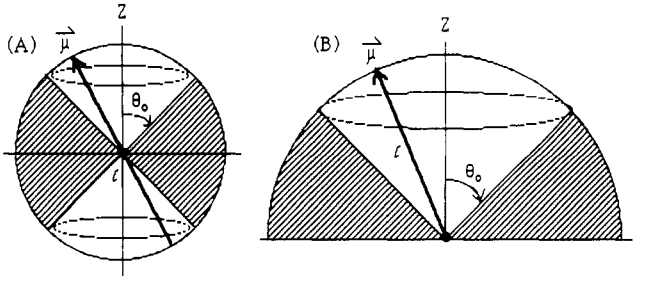

Figure 14. A schematic picture shows two different kinds of chromophore rotating in a polymer matrix. (A) If there is no interaction between the chromophore and the polymer chains, the chromophore is rotating around its geometric center. (B) The chromophore is rotating around its one end which is bound to the polymer chain.

Once the average apparent angle is determined from experimental data, the real wedge angle can be calculated by solving eq 34. The values of $\langle\theta_a\rangle$ and θ_0 are listed in Table 2.

In case B, the boundary conditions are not the same as those defined before:

$$\text{B.C.1:} \quad \left.\frac{\partial p(\theta,t)}{\partial\theta}\right|_{\theta=\alpha-\theta_0} = 0 \tag{35}$$

and

$$\text{B.C.2:} \quad \left.\frac{\partial p(\theta,t)}{\partial\theta}\right|_{\theta=\alpha+\theta_0} = 0 \tag{36}$$

Because the θ-domain no longer contains the regular singular point, the Frobenius series (eq 9) is inappropriate in deriving the solution which satisfies the above B.C.'s. The numerical work becomes more complex because the probability density p must be calculated at all possible tilted angles α and averaged to obtain the orientational order. However, since the orientations of these cones are much further away from the Z-axis than those in case A, the chromophores located within these cones will be less aligned and contribute little to the total observed $\chi^{(2)}$ signal.

If there is no interaction between the chromophore and the polymer matrix, the chromophore should rotate around its geometrical center provided the dipole moment, μ, is along the major geometrical axis of the chromophore and the donor and acceptor groups are at both ends. In this case, denoted as case 1, the chromophore is wobbling within two cones as shown in Figure 14A. The total volume of the two cones is calculated by

$$V_c = 2\int_0^{\theta_0}\int_0^{\ell/2}\int_0^{2\pi} r^2 \sin\theta\, d\phi\, dr\, d\theta + V_e = \frac{\pi}{6}\ell^3(1 - \cos\theta_0) + V_e \tag{37}$$

where ℓ is the axial length of the chromophore and r is the radius of the cross section of the chromophore. For DANS, ℓ and r are equal to 14.2 and 2.15 Å, respectively (calculated using van der Waals volumes). V_e is the "extra volume" swept by the chromophore and equals zero if the radius r is zero. The detailed calculation of V_e is given in the Appendix.

If there is some interaction which binds the chromophore, for example, at one end to the polymer chain (such as hydrogen bonding), then the chromophore can be visualized as wobbling around the fixed end and rotating

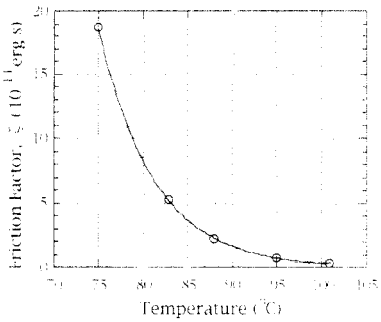

Figure 15. Temperature dependence of the friction factor, ζ, for the PMMA + 4 wt % DANS system.

within one cone (case 2, Figure 14B).[54] The cone volume becomes

$$V_c = \int_0^{\theta_0}\int_0^{\ell}\int_0^{2\pi} r^2 \sin\theta \, d\phi \, dr \, d\theta + V_e = \frac{2\pi}{3}\ell^3(1 - \cos\theta_0) + V_e \quad (38)$$

The volume of the space which the chromophores can rotate into is then given by

$$V_0 = V_c - v_c \quad (39)$$

where v_c is the volume of the chromophore and is equal to 207 Å^3 for DANS (calculated using van der Waals volumes). If V_0 is viewed as the volume which is not occupied by either the polymer or the chromophores, it can represent the apparent mean free volume of the doped polymer system for a first-order approximation. The value of V_0 is useful in characterizing the rotational freedom of chromophores in a polymer matrix. Table 2 gives the values of V_0, as well as the corresponding values of V_c and θ_0, at different temperatures for PMMA + 4 wt % DANS films.

It can be seen from eqs 37 and 38 that the cone volume in case 2 is larger than that in case 1 if θ_0 is the same for both cases. This indicates that in case 2 more free volume is needed than in case 1 for chromophores to achieve the same orientational order ($\langle\cos^3\theta\rangle$, which is a function of θ_0). The physical significance is that the poling temperature must be higher to create more free volume (or local mobility) for the "host-bound" chromophores to obtain the same $\chi^{(2)}$ signal, which can be obtained at a lower temperature for the unbound chromophores. If the cone volume in each case is the same, then θ_0 of case 2 will be smaller than that of case 1. That means although the free volume is the same, the polymer restriction (which is expressed in terms of θ_0) becomes more efficient in case 2 than in case 1. This implies θ_0 may be a better index than free volume in describing the effect of the polymer restriction on the chromophore rotational dynamics.

Local Viscosity. Figure 15 shows the temperature dependence of the rotational friction factor, ζ, following poling. The friction factor is defined by the Nernst–Einstein equation:

$$\zeta \equiv \frac{k_B T}{D} \quad (40)$$

where $k_B T$ is the thermal energy and D is the rotational diffusion coefficient. It is found that the ζ–temperature curve shown in Figure 15 can be described by an exponential curve:

$$\zeta = \zeta_0 \exp\left(-\frac{T - T_g}{T_0}\right) \quad (41)$$

where ζ_0 and T_0 are fitting parameters. For the PMMA + 4 wt % DANS system (T_g = 88 °C), the values of ζ_0 and T_0 are 2.26 × 10^{-11} erg s and 6.17 K, respectively.

Perrin[55] developed an equation which relates the friction factor and the viscosity for an ellipsoidal particle rotating in a viscous medium:

$$\zeta = 4\eta v_c \frac{s^4 - 1}{s^2}\left(-1 + \frac{2s^2 - 1}{2s(s^2 - 1)^{1/2}} \ln\left(\frac{s + (s^2 - 1)^{1/2}}{s - (s^2 - 1)^{1/2}}\right)\right)^{-1}, \quad \text{for } s > 1 \quad (42)$$

where η is the viscosity of the surroundings and v_c is the volume of the rotating particle. The parameter s is the shape factor, which is defined as the ratio of the length of the longitudinal axis to that of the transverse axis of the rotating particle. For DANS, v_c is 207 Å^3 and s is equal to 3.3.

Assuming that the doped chromophores are allowed to rotate within a local low-density area with a viscosity η in a polymer matrix, then eq 42 is applicable. The relationship between the friction factor and the viscosity for the PMMA + DANS system is therefore given by

$$\eta = 3.07 \times 10^{20}\zeta \quad (43)$$

where the units of η and ζ are poise and erg seconds, respectively. Substituting eq 43 into eq 41, the temperature dependence of η is given by a single exponential equation:

$$\eta = \eta_0 \exp\left(-\frac{T - T_g}{T_0}\right) \quad (44)$$

where η_0 equals 6.94 × 10^9 P and T_0 is 6.17 K.

Equation 44 is similar to the Doolittle equation:

$$\eta = A \exp\left(B\frac{v - v_f}{v_f}\right) \quad (45)$$

where v is the specific volume and v_f is the free volume.[56,57] A and B are material parameters. Williams, Landel, and Ferry (WLF)[58] assumed that the free volume increases linearly with temperature and proposed an empirical equation:

$$v_f = v_g(f + \Delta\alpha(T - T_g)) \quad (46)$$

where v_g is the specific volume at T_g and $\Delta\alpha = (\alpha_l - \alpha_g)$ is the excess thermal expansion coefficient of the liquid with respect to the glass. f is the fraction of free volume at T_g and was taken to be 0.025 by the authors. Substituting eq 46 into the Doolittle equation, the temperature dependence of viscosity is then described by

$$\eta = A \exp\left(B\frac{\alpha_g(T - T_g) + (1 - f)}{\Delta\alpha(T - T_g) + f}\right) \quad (47)$$

The η–temperature curves fitted using eqs 44 and 47, as well as the data points calculated from the rotational dynamic model, are shown in Figure 16. The errors between the curves and the data points are less than 0.1%. Parameters A and B in eq 45 are found to be 3.46 × 10^5 and 0.244, respectively, if η is in units of poise. The thermal expansion coefficients, α_l and α_g, of the polymer system are assumed to be affected little by the dopant and

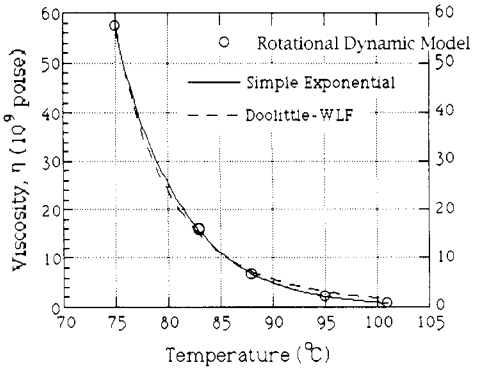

Figure 16. Viscosity (η)–temperature curves for the (- - -) PMMA + 4 wt % DANS system fitted using eq 44 ((—) simple exponential) and eq 47 Doolittle–WLF). The data points (○) were calculated from the rotational dynamic model.

Table 3. Comparison of the Free Volumes Predicted by the WLF Equation (v_f) and the Rotational Dynamic Model (V_0)

	T (°C)				
T (°C)	75	83	88	95	101
v_f (Å^3)	202	223	245	266	276
V_0 (Å^3)	462	491	1293	1293	1293

approximately equal to 5.75×10^{-4} and 2.55×10^{-4} K^{-1}, respectively.[59,60] The free volume fraction, f, is found to be 0.024, which is close to that proposed by the WLF equation. It can be seen in Figure 16 that the viscosity–temperature behavior predicted by the model is consistent with that described by the Doolittle–WLF equation. Both curves show a non-Arrhenius dependence of the viscosity on temperature.

However, the underlying physical significances of the Doolittle–WLF equation and the rotational dynamic model are different. Originally, the Doolittle or the WLf equations were developed empirically to explain the temperature dependence of viscosity or the change in viscoelastic properties of polymers above T_g. Therefore, they are valid at temperatures above T_g. The values of viscosity calculated by the Doolittle–WLF equation are taken as an indication of the friction encountered by the polymer chains in global motion. When the temperature is below T_g, the global motion of the polymer chains is greatly decreased and becomes undetectable on the regular laboratory time scale. The Doolittle or WLF equations fail below T_g because the global motion of the polymer chains no longer obeys the behavior at liquid state. However, the model in this work is developed to describe a small-scale motion in a sub-T_g polymer system. The viscosity obtained by the model, therefore, represents the resistance of the local motion in polymers.

The consistency of the model and the Doolittle–WLF equation implies that although the large-scale motion is dramatically impeded below T_g, there is some area where the local motion is allowed to occur and behaves just like that above T_g (or there exists some local motion which is so mobile that it results in a low viscosity area whose property is similar to that of the liquid state).

Equation 46 gives an empirical definition of free volume, v_f, proposed by WLF. The values of v_f and V_0 (the local free volume computed from the rotational Brownian model) are listed in Table 3. The difference between the values of v_f and V_0 comes from the neglecting of the plasticization in a doped polymer system in the calculation of v_f. The values of the parameters in eq 46, including the thermal expansion coefficients and the specific volume, are taken as the ones of pure PMMA. Therefore, the value of v_f is close to that of a pure polymer rather than the doped system. It can be seen that the extra volume introduced by the chromophore is large ($V_0 - v_f$) and gives rise to a significant decreasing of T_g in the doped polymer (pure PMMA: T_g = 105 °C; PMMA + 4 wt % DANS: T_g = 88 °C).

Another difference of v_f and V_0 comes from their definition. The value of v_f indicates the average free volume in the polymer bulk. However, V_0 is referred to the local free volume surrounding the chromophore. This also suggests that the model is more sensitive in describing the local motion which cannot be predicted by the WLF equation.

Conclusions

A dynamic model which describes the rotational Brownian motion of NLO chromophores in a poled polymer has been developed in this work. This model exhibits the ability to reproduce the time dependence of the $\chi^{(2)}$ signal during the following poling. With the information obtained from the model, the $\chi^{(2)}$ relaxation behavior, as well as the local mobility in NLO polymers, can be understood and quantified.

The temperature for obtaining the maximum $\chi^{(2)}$ value is observed at the glass transition temperature for the PMMA + DANS system. The magnitude of $\chi^{(2)}$ is governed by three major mechanisms—the rotational Brownian motion, electric field effects, and polymer restrictions—which dominate at different temperatures. There exists a temperature which optimizes these factors and gives a maximum value of $\chi^{(2)}$. At the glass transition temperature, the polymer restriction reaches its minimum; it therefore gives a suitable environment for the applied electric field to orient the chromophores efficiently.

The residual electric field effects on the $\chi^{(2)}$ relaxation following corona poling have been examined by measuring the second harmonic intensity and the surface voltage simultaneously. The residual electric field has been found to increase the temporal stability of the $\chi^{(2)}$ signal. With the numerical method introduced in this work, the remaining surface voltage has been separated to reveal the contribution of the rotational Brownian motion and polymer restriction to the $\chi^{(2)}$ relaxation. The $\chi^{(2)}$ signal shows a decay rate closer to that of average electric torque rather than that of surface voltage. The polymer restrictions (below T_g), the rotational Brownian motion (near T_g), and the charge injection (above T_g) are believed to result in the deviation of $\chi^{(2)}$ relaxation from surface voltage decay.

The magnitude of the rotational diffusion coefficient of DANS doped in PMMA has been calculated ranging from 10^{-4} to 10^{-2} s^{-1} at temperatures 10 °C below to 10 °C above the glass transition temperature. It has also been found that the rotational diffusion coefficients during and following corona poling are of the same order but have different values after the remaining surface voltage effect is deconvoluted. It is suspected that the field-induced bulk charges and the thermally excited charge injection may contribute to this difference.

The application of the rotational diffusion model in estimating the local free volume and viscosity has been illustrated. The polymer restriction on rotating chromophores was modeled as a rigid cone, which confines the rotational motion in a limited space. The cone volume, or the wedge angle of the cone, therefore, represents the local free volume or local mobility of the polymer matrix around the chromophores. It has also been shown that the wedge angle may be a better index of the local mobility

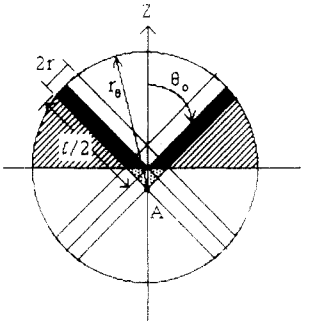

Figure 17. Rotation of a long rodlike particle (length = ℓ, radius of cross section = r) around its geometric center with a maximum polar angle θ_0.

than the cone volume when there is an interaction between the guest and the host.

The rotational friction factor of DANS doped in PMMA has been calculated and related to the local viscosity. The local viscosity–temperature behavior predicted by this model is found to be consistent with the Doolittle–WLF equation. This implies the superior ability of the SHG technique and the rotational dynamic model in probing and quantifying the local or small-scale mobility in polymers below T_g.

Acknowledgment. We are deeply indebted to the Engineering Research Foundation (AFOSR), the National Science Foundation, and the Society of Photo-Optical Instrumentation Engineers (L.-Y.L.) for financial support.

Appendix

A rigid, rod-like (cylindrical) particle is rotating around its geometric center in space without any translational movement. The rotation of this particle is independent of the azimuthal angle and is restricted within a polar angle θ_0. θ_0 is defined as the angle measured from the polar axis to the geometric axis of the particle. The space which can be swept by the particle forms the shape as shown in Figure 17. If the length of the particle is ℓ and the radius of its cross section is r, then the volume of the swept space is given by

$$V_c = 2\left[\int_0^{2\pi} r' \sin\theta \, d\phi \int_0^{\theta_0} r' \, d\theta \int_0^{r_\theta} dr' - \frac{\pi}{3}\frac{r^3}{\sin\theta_0 \cos^2\theta_0}\right] \tag{A.1}$$

where r', θ, and ϕ are the radial, polar, and azimuthal variables, respectively. The cubic term of r in eq A.1 indicates the volume which is overcounted in the integral (the dotted area in Figure 17). The parameter r_θ is a θ-dependent distance which is measured from point A to the circumference swept by the end point of the particle. The relationship between r_θ and θ is

$$\cos\theta = \frac{r_\theta^2 - (L^2 - d_0^2)}{2d_0 r_\theta} \tag{A.2}$$

where

$$L = \frac{\ell}{2} + r\cot\theta_0 \tag{A.3}$$

and

$$d_0 = \frac{r}{\sin\theta_0}(1 - \cos\theta_0) \tag{A.4}$$

The integral part of eq A.1 is integrated as follows:

$$\int_0^{2\pi} r' \sin\theta \, d\phi \int_0^{\theta_0} r' \, d\theta \int_0^{r_\theta} dr' = \frac{-2\pi}{3}\int_{\theta=0}^{\theta=\theta_0} r_\theta^3 \, d\cos\theta \tag{A.5}$$

According to eq A.2 and defining

$$y \equiv \frac{r_\theta^2 - (L^2 - d_0^2)}{r_\theta} \tag{A.6}$$

r_θ can be rewritten in terms of y as

$$r_\theta = \frac{1}{2}(y + (y^2 + 4c)^{1/2})^3 \tag{A.7}$$

where c is defined as $(L^2 - d_0^2)$. Equation A.5 can be expressed as

$$\text{eq A.5} = \frac{-\pi}{24 d_0}\int_{\theta=0}^{\theta=\theta_0}(y + (y^2 + 4c)^{1/2})^3 \, dy \tag{A.8}$$

After performing a series of integrations, the final result is

$$\text{eq A.5} = \frac{-\pi}{24 d_0}\{y^4 + 6cy^2 + y(y^2 + 4c)^{3/2}\}_{\theta=0}^{\theta=\theta_0} \tag{A.9}$$

Substituting eqs A.2–A.4 and A.6–A.9 into eq A.1, V_c is given by

$$V_c = \frac{2\pi}{3}\left\{\frac{2(1 - \cos\theta_0)^3(1 + \cos^2\theta_0)}{\sin\theta_0} r^3 + 3\left[\frac{\ell}{2} + \frac{r}{\sin\theta_0}(1 + 2\cos\theta_0)\right]\left[\frac{\ell}{2} + \frac{r}{\sin\theta_0}\right]\sin\theta_0(1 - \cos\theta_0) r + 2\left[\left(\frac{\ell}{2} + r\cot\theta_0\right)^3 - \cos\theta_0\left[\left(\frac{\ell}{2} + r\cot\theta_0\right)^2 - \left(\frac{r}{\sin\theta_0}\right)^2(1 - \cos\theta_0)^3\right]^{3/2}\right]\right\} \tag{A.10}$$

V_c can be viewed as the summation of the inside cone volume (blank part in Figure 17) and the extra volume swept by the particle around the edge of the inside cones (the dark part in Figure 17). The volume of the inside cones can be calculated as

$$V_{is} = 2\int_0^{\theta_0}\int_0^{\ell/2}\int_0^{2\pi} r^2 \sin\theta \, d\phi \, dr \, d\theta = \frac{\pi}{6}\ell^3(1 - \cos\theta_0) \tag{A.11}$$

Thus the extra volume V_e can be derived by subtracting V_{is} from V_c.

If the shape of the rotating particle is ellipsoidal rather than rodlike (cylindrical), then the value of V_e is about $\pi/4$ times that of V_e for a rodlike particle. Therefore, the volume swept by an ellipsoidal particle can be approximated by

$$V_{c,ellipsoid} \cong V_{is} + \frac{\pi}{4}V_{e,rod} \tag{A.12}$$

If the particle is rotating around one of its ends, the value of V_c is calculated by substituting ℓ rather than $\ell/2$ into eq A.10 and dividing the result by 2.

References and Notes

(1) Malouin, C.; Galarneau, P.; Lessard, R. A. In *Organic Molecules for Nonlinear Optics and Photonics*; Messier, J., *et al.*, eds.; Kluwer Academic: Dordrecht, 1991; p 513.

(2) Burland, D. M.; Miller, R. D.; Reiser, O.; Twieg, R. J.; Walsn, C. A. *J. Appl. Phys.* **1992**, *71*, 410.
(3) Gauglitz, G.; Ingenhoff, J. *Ber. Bunsenges. Phys. Chem.* **1991**, *95*, 1558.
(4) Hikita, M.; Shuta, Y.; Amano, M.; Yoshimura, R.; Tomaru, S.; Kozawaguchi, H. *Appl. Phys. Lett.* **1993**, *63*, 1161.
(5) Natansohn, A.; Rochon, P.; Gosselin, J.; Xie, S. *Macromolecules* **1992**, *25*, 2268.
(6) Hornak, L. A., Ed. *Polymers for Lightwave and Integrated Optics*; Marcel Dekker: New York, 1992.
(7) Baek, W. S.; Lee, H. *J. Appl. Phys.* **1990**, *67*, 1194.
(8) Lytel, R.; Lipscomb, G. F.; Kenney, J. T.; Ticknor, A. J. *SPIE, Optical Enhancements to Computing Technology* **1991**, 1563.
(9) Prasad, P. N.; Williams, D. J. *Introduction to Nonlinear Optical Effects in Molecules and Polymers*; John Wiley & Sons: New York, 1991.
(10) Williams, D. J., Ed. *Nonlinear Optical Properties of Organic Molecules and Polymeric Materials*; ACS Symposium Series 233; American Chemical Society: Washington, DC, 1983.
(11) Sohn, J. E.; Singer, K. D.; Kuzyk, M. G. In *Polymers for High Technology, Electronics and Photonics*; Bowden, M. J.; Turner, S. R., Eds.; ACS Symposium Series 346; American Chemical Society: Washington, DC, 1987.
(12) Thackara, J. I.; Lipscomb, G. F.; Stiller, M. A.; Ticknor, A. J.; Lytel, R. *Appl. Phys. Lett.* **1988**, *52*, 1031.
(13) Meredith, G. R.; van Dusen, J.; Williams, D. J. *Macromolecules* **1982**, *15*, 1385.
(14) Williams, D. J. *Angew. Chem., Int. Ed. Engl.* **1984**, *23*, 690.
(15) Singer, K. D.; Sohn, J. E.; Lalama, S. J. *Appl. Phys. Lett.* **1986**, *49*, 248.
(16) de Martino, R. N.; Yoon, H. N. US Patent 4808332, 1989.
(17) Hampsch, H. L.; Yang, J.; Wong, G. K.; Torkelson, J. M. *Macromolecules* **1988**, *21*, 526.
(18) Kuzyk, M. G.; Moore, R. C.; King, L. A. *J. Opt. Soc. Am. B* **1990**, *7*, 64.
(19) Teraoka, I.; Jungbauer, D.; Reck, B.; Yoon, D. Y.; Twieg, R.; Willson, C. G. *J. Appl. Phys.* **1991**, *69*, 2568.
(20) Singer, K. D.; King, L. A. *J. Appl. Phys.* **1991**, *70*, 3251.
(21) Lindsay, G. A.; Henry, R. A.; Hoover, J. M.; Knoesen, A.; Mortazavi, M. A. *Macromolecules* **1992**, *25*, 4888.
(22) Dhinojwala, A.; Wong, G. K.; Torkelson, J. M. *Macromolecules* **1993**, *26*, 5943.
(23) Hampsch, H. L.; Yang, J.; Wong, G. K.; Torkelson, J. M. *Macromolecules* **1990**, *23*, 3640.
(24) Man, H. T.; Yoon, H. N. *Adv. Mater.* **1992**, *4*, 159.
(25) McConnell, J. *Rotational Brownian Motion and Dielectric Theory*; Academic Press: New York, 1980.
(26) Warchol, M. P.; Vaughan, W. E. *Adv. Mol. Relax. Interact. Proc.* **1978**, *13*, 317.
(27) Wang, C. C.; Pecora, R. *J. Chem. Phys.* **1980**, *72*, 5333.
(28) Tool, A. M. *J. Am. Ceram. Soc.* **1946**, *29*, 240.
(29) Kovacs, A. J.; Aklonis, J. J.; Hutchinson, J. M.; Ramos, A. R. *J. Polym. Sci., Polym. Phys. Ed.* **1979**, *17*, 1097.
(30) Williams, D. J. *Polymer Science and Engineering*; Prentice-Hall: Englewood Cliffs, NJ, 1971.
(31) Rudin, A. *The Elements of Polymer Science and Engineering*; Academic Press: New York, 1982.
(32) McCrum, N. G.; Read, B. E.; Williams, G. *Anelastic and Dielectric Effects in Polymeric Solids*; Dover Publications: New York, 1991.
(33) Dickinson, E.; Allison, S. A.; McCammon, J. A. *J. Chem. Soc., Faraday Trans. 2* **1985**, *81*, 591.
(34) Benoit, H. *Ann. Phys.* **1951**, *12*, 561.
(35) Happel, J.; Brenner, H. *Low Reynolds Number Hydrodynamics*; Prentice-Hall: Englewood Cliffs, NJ, 1965.
(36) Belmonte, A. P.; Martinez, M. C. L.; de la Torre, J. G. *J. Phys. Chem.* **1991**, *95*, 952.
(37) Martinez, M. C. L.; Belmonte, A. P.; de la Torre, J. G. *J. Phys. Chem.* **1991**, *95*, 5661.
(38) Wu, J. W. *J. Opt. Soc. Am. B* **1991**, *8*, 142.
(39) Greenberg, M. D. *Foundations of Applied Mathematics*; Prentice-Hall: Englewood Cliffs, NJ, 1978.
(40) Hobson, E. W. *Spherical and Ellipsoidal Harmonics*; Cambridge University Press: Cambridge, London, 1931.
(41) Ramkrishna, D.; Amundson, N. R. *Linear Operator Methods in Chemical Engineering*; Prentice-Hall: Englewood Cliffs, NJ, 1985.
(42) Giacometti, J. A.; Oliveira, O. N., Jr. *IEEE Trans. Elec. Insul.* **1992**, *27*, 924.
(43) Milner, S.; Douglas, J., private communications.
(44) Dao, P. T.; Williams, D. J. *J. Appl. Phys.* **1993**, *73*, 2043.
(45) Ieda, M.; Sawa, G.; Shinohara, U. *Jpn. J. Appl. Phys.* **1967**, *6*, 793.
(46) Debye, P. *Ber. Dtsch. Phys. Ges.* **1913**, *15*, 777.
(47) Reiser, A.; Lock, M. W. B.; Knight, J. *Trans Faraday Soc.* **1969**, *65*, 2168.
(48) von Seggern, H. *J. Appl. Phys.* **1979**, *50*, 2817.
(49) von Seggern, H. *J. Appl. Phys.* **1981**, *52*, 4081.
(50) Weiss, D. S. *J. Imaging Sci.* **1990**, *34*, 132.
(51) Das-Gupta, D. K. *IEEE Trans. Elec. Insul.* **1992**, *27*, 909.
(52) Kasap, S. O. *J. Phys. D: Appl. Phys.* **1992**, *25*, 83.
(53) Andry, P.; Filion, Y.; Perlman, M. M. *J. Appl. Phys.* **1992**, *71*, 750.
(54) Fu, C. Y. S.; Lackritz, H. L.; Priddy, D. B., Jr.; Lyle, G. D.; McGrath, J. E., submitted.
(55) Perrin, F. *J. Phys. Radium* **1934**, *VII*.
(56) Doolittle, A. K. *J. Appl. Phys.* **1951**, *22*, 1471.
(57) Doolittle, A. K. *J. Appl. Phys.* **1952**, *23*, 236.
(58) Williams, M. L.; Landel, R. F.; Ferry, J. D. *J. Am. Chem. Soc.* **1955**, *77*, 3701.
(59) Hennig, J. Diplomarbeit TH Darmstadt, 1961.
(60) Loshaek, S. *J. Polym. Sci.* **1955**, *15*, 391.